Combustion and Flame 160 (2013) 1650–1656

Contents lists available at SciVerse ScienceDirect

Combustion and Flame

journal homepage: www.elsevier.com/locate/combustflame

Sooting behaviour of *n*-heptane laminar diffusion flames at high pressures

Ahmet E. Karataş, Gorngrit Intasopa, Ömer L. Gülder *

Institute for Aerospace Studies, University of Toronto, 4925 Dufferin Street, Toronto, ON, Canada M3H 5T6

ARTICLE INFO

Article history:
Received 25 December 2012
Received in revised form 13 February 2013
Accepted 5 March 2013
Available online 3 April 2013

Keywords:
High-pressure soot
n-Heptane
Soot yield
Diffusion flames
Liquid fuel

ABSTRACT

The effect of pressure on sooting behaviour of *n*-heptane is studied in co-flow *n*-heptane/air laminar diffusion flames at pressures above atmospheric in a high pressure combustion chamber. The fuel is diluted with either nitrogen or helium to keep a non-smoking flame at elevated pressures, and the selected fuel mass flow rate of *n*-heptane provided diffusion flames in which the soot was completely oxidized within the visible flame envelope. The flame stability proved to be a challenge and stable flames were possible only at certain pressures for a sufficiently long duration to permit measurements. The soot volume fractions and temperatures were measured by spectral soot emission as a function of pressure for nitrogen-diluted *n*-heptane flames at 2, 5 and 7 atm. For helium-diluted *n*-heptane flames, line of sight soot emission data at 3, 4, and 5 atm are presented at two heights above the burner exit. Comparison of limited nitrogen-diluted *n*-heptane data to previous measurements of soot yields indicate that soot formation in diffusion flames of *n*-heptane seems to be slightly more sensitive to pressure than that in aliphatic gaseous fuel diffusion flames within the pressure range considered in this work.

1. Introduction

The highly complex nature of hydrocarbon diffusion flames poses challenges in unraveling the underpinning physical and chemical mechanisms of soot formation and oxidation. As a result only a few principles are firmly established mostly for atmospheric gaseous fuel diffusion flames. For liquid fuels, we still rely on smoke point of the fuel or sooting index for practical applications due to a lack of full understanding of the effects of the various operating conditions on the soot formation process [1,2]. Earlier efforts to link the smoke point and sooting tendency of liquid fuels to chemical structure of the fuel were successful [3,4], and they provided scaling information for further studies on sooting propensities of hydrocarbons, see e.g., [5].

The overall reaction rate in hydrocarbon–air combustion (i.e., combustion intensity or heat release per unit volume) scales approximately with the square of the operating pressure, thus the relative size of the combustion device gets smaller as the operating pressure is increased for a required power output. In spite of the fact that most combustion devices used for transportation operate at elevated pressures (e.g., aircraft gas turbines up to 40 atm, diesel engines exceeding 100 atm), our understanding of soot formation at these pressures is not at a desirable level, and there is a lack of bench-mark experimental data and complementary predictive models [6].

In practical diffusion combustion systems, such as diesel and aircraft gas turbine engines, and in fires the combustion is turbulent. However, the high level of intermittency and relatively shorter residence times associated with turbulent diffusion flames limit the experimental accessibility of these flames and make it difficult to track combustion events like soot formation. Further the non-homogeneous nature of turbulent diffusion flames makes it challenging to isolate parameters that affect soot formation and oxidation. One of the most widely used approximations to exploit similarities between laminar and turbulent diffusion flames is to use the laminar flamelet concept (or approaches based on flamelets), which provides a tractable flame model [7–9]. For this reason, most of the soot studies at elevated pressures have been done in laminar diffusion flames of co-flow type, which permit to isolate the parameters that influence the soot formation process.

Experimental research in laminar diffusion flames at pressures above atmospheric have been held back by the challenges in designing an experimental apparatus and in operating instruments that require accessibility for intrusive and non-intrusive measurement techniques [7]. In addition, the stability of laminar diffusion flames, especially originating from buoyancy effects, becomes an important issue at elevated pressures due to the increase in Grashoff number, which scales with the square of pressure. These impediments have limited the number and the extent of

* Corresponding author. Fax: +1 416 667 7799.
E-mail address: ogulder@utias.utoronto.ca (Ö.L. Gülder).

0010-2180/$ - see front matter © 2013 The Combustion Institute. Published by Elsevier Inc. All rights reserved.
http://dx.doi.org/10.1016/j.combustflame.2013.03.008

experimental soot studies in laminar diffusion flames at elevated pressures [10].

Available high-pressure experimental data on soot in combustion literature are limited to laminar gaseous diffusion flames. Flower and Bowman [11] studied laminar diffusion flames of ethylene at a pressure range of 1–10 atm, by measuring line-of-sight integrated soot volume fractions and temperatures along the flame centreline. They report a pressure scaling of the maximum integrated soot volume fraction with an exponent of 1.2 ± 0.1 from atmospheric to 10 atm pressure for ethylene diffusion flames. Measurements of Lee and Na [12] indicate a similar pressure scaling for the maximum soot volume fraction with an exponent of 1.26 in laminar ethylene flames from 2 atm to 4 atm. McCrain and Roberts [13] measured path integrated and local soot volume fractions by line-of-sight attenuation and laser-induced incandescence, respectively. Their measurements covered a pressure range of 1–25 atm in methane flames and 1–16 atm in ethylene diffusion flames. First detailed data sets of radially resolved soot concentration and soot temperature measurements at elevated pressures up to 40 atm were reported by Thomson et al. [14] and up to 60 atm by Joo and Gülder [15], in laminar diffusion flames of methane using soot emission spectroscopy. Measurements by Bento et al. [16] on laminar diffusion flames of propane covered the pressure range from atmospheric to 7.3 atm, and their results were comparable to the low pressure range reported in [14]. Similar experimental studies in ethane laminar diffusion flames up to 33 atm [17] and in nitrogen-diluted ethylene diffusion flames up to 35 atm [18] were recently reported. Most recently, Gülder et al. [19] demonstrated that the available high pressure soot yield data from aliphatic gaseous diffusion flames display a unified dependence on pressure when the soot yield is properly normalized. Soot yield seems to reach a plateau asymptotically, as the pressure is increased, around the critical pressure of the fuel [19].

As briefly reviewed in the previous paragraph, information on soot formation processes in laminar diffusion flames at higher pressures is limited to ethylene, methane, ethane and propane flames [10–18,20]. There is no data available on the sooting behaviour of liquid fuels in tractable laminar diffusion flames at pressures above atmospheric: most data, if not all, are at atmospheric pressure. The only study with a liquid fuel at pressures above atmospheric has been reported recently [21]. The effects of small amounts of m-xylene (up to 5% of fuel carbon coming from m-xylene as a perturbation to a base flame) on aromatic species and soot were studied in a nitrogen-diluted ethylene flame between 1 and 5 atm. Their results indicate that the observed increase in soot and aromatic species are about first order with respect to amount of m-xylene added to the flame [21].

Liquid fuels currently used in air and ground transportation are mostly petroleum based, and they contain hundreds of different hydrocarbons with various properties dependent on the source and the refining process. The main objective of the research reported in this paper was to determine the sooting behaviour of a co-flow *n*-heptane/air laminar diffusion flame at pressures above atmospheric. Soot and temperature measurements in nitrogen-diluted *n*-heptane flames are presented for pressures up to 7 atm. Also presented are the spectral soot emission measurements in helium-diluted *n*-heptane flames for pressures up to 5 atm. Of course *n*-heptane is not a commercial transportation fuel but is thought to be a good surrogate or surrogate fuel component. In some studies with liquid fuels, *n*-heptane is considered as a good pure hydrocarbon that is representative of liquid transportation fuels to a certain extent. Also it is one of the two primary reference fuels for octane rating of spark-ignition engine fuels. Further, there have been several recent studies on oxidation, pyrolysis, chemical kinetics, and ignition delay of *n*-heptane at various pressures, see for example [22–24].

2. Experimental method

The experimental high pressure combustion chamber used in this study is described in detail in [14–17]. The design pressure of the chamber is about 110 atm, and its internal diameter and internal height are 0.24 m and 0.6 m, respectively. Optical access into the chamber is through three ports at 0°, 90°, and 180° locations allowing line-of-sight measurements as well as 90° scattering and imaging experiments. A schematic of the experimental setup is given in Fig. 1.

The dilution and evaporation of the liquid fuel is completed outside the pressure chamber. A syringe pump (Teledyne Series D 500D) is used to feed the liquid fuel into a heated evaporation chamber. The fuel evaporation and mixing chamber is a small volume (about 4×10^{-5} m^3) high-pressure vessel that has a pressure rating of 122 atm, and denoted as the evaporator in Fig. 1. Liquid fuel and heated carrier gas, nitrogen or helium, are injected into this heated evaporation chamber through a co-flow injector. Central liquid fuel nozzle has a diameter of 0.15 mm and co-flow carrier gas flows through an 8 mm nozzle. Fully evaporated and diluted fuel is then directed to the burner through a tube heated by wrap-around cable heaters to avoid condensation. A thermocouple is placed into the flow just before the burner to control the pre-combustion mixture temperature. For *n*-heptane experiments, the fuel evaporation chamber and the diluted fuel line to the burner were kept at about 525 K by temperature controllers.

The burner used in this study is different in internal design from the burner used in our previous studies with gaseous fuels [14–17]. The new burner allows liquid fuel mixture as well as gaseous fuel mixture experiments. The basic dimensions of the new annular co-flow burner were influenced by the design of Miller and Maahs [25] and the existing gas burner that provided excellent flame stability in our previous studies with gaseous fuels. The unique design also allows direct and simultaneous introduction of liquid and gaseous fuels to the burner. An important component of the burner is the fuel nozzle (316L stainless steel) with a sintered metal foam insert (nickel–chromium, RETINET foam grade 80). The exit diameter

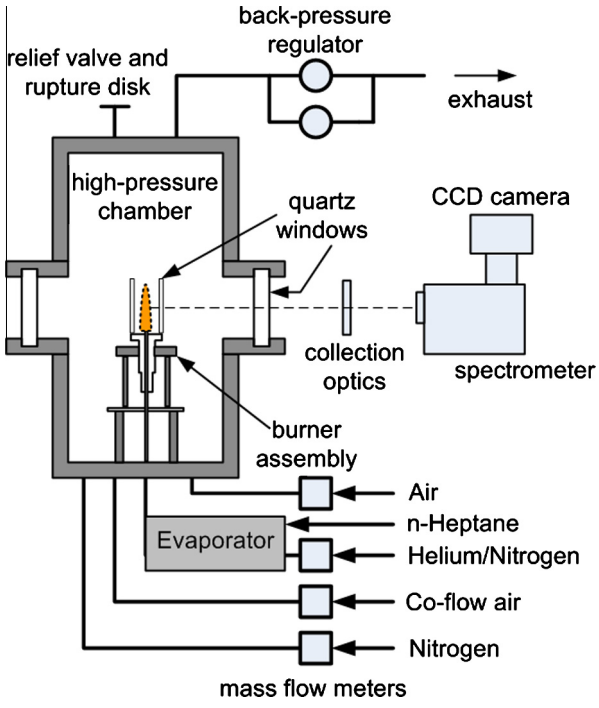

Fig. 1. A schematic view of the experimental setup.

of the fuel nozzle is precision machined to 3.0 mm. The air nozzle diameter is 25.4 mm. A detailed drawing of the burner is shown in Fig. 2. The thermal feedback from the stabilized flame prevents any possible condensation of the pre-vaporized fuel around the metal foam. The sintered foam acts as a thermally conductive element to transfer the heat from the flame upstream and allows the passage of the pre-vaporized fuel.

The theory and overall experimental layout of the spectral soot emission diagnostic (SSE) are described previously [26]. In SSE, line-of-sight radiation emission from soot is measured along chords through the flame. A series of emission projections at a given height in the flame can be inverted to obtain radially resolved emission rates from which temperature and soot volume fraction can be determined when soot optical properties are known [27]. The emitted radiation from soot first passes through an adjustable aperture and lens unit. For the current study an aperture diameter of about 6.2 mm and associated f-number of f/48 was used. The lens selected for this study is an achromatic doublet lens with a focal length of 300 mm. The lens has an antireflective coating, effective within the wavelength range of 650–1050 nm. The purpose of the lens is to image the flame radiation onto the entrance slit of the spectrometer. The lens is positioned to produce a 1:1 image. The entrance to the spectrometer contains two slits: the vertical slit is approximately 25 μm in width and the horizontal slit is approximately 290 μm in height. The slit sizes play a role in the resulting spatial resolution of the collected data [26].

The spectrometer is an imaging Czerny-Turner spectrometer that internally uses aspheric mirrors. The spectrometer grating used for this task has a blaze wavelength of 775 nm and is manufactured with 300 groves/mm. The spectrometer has a dispersion of approximately 18.84 nm/mm. Soot emission is measured over a wavelength range of 690–945 nm. The total array size of the CCD is 1340 × 400 pixels. However, due to the restricted size of the entrance slit, a region of interest of size 1340 × 80 pixels was selected. Combined with the previously mentioned spectrometer and grating, the CCD camera is capable of capturing an approximate wavelength spread of 505 nm across the camera array, providing a spectral step size of 0.377 nm/pixel. Knife-edge scans across a diffuse light source located at the object plane indicated a horizontal spatial resolution of 70 μm over the depth of field defined by the burner nozzle exit diameter. The vertical spatial resolution was inferred to be approximately 290 μm. To calibrate the spectral axis of the CCD array a pencil style neon calibration lamp was used. The system is calibrated for radiation intensity using a filament lamp, with a calibration traceable to NIST, placed inside the chamber.

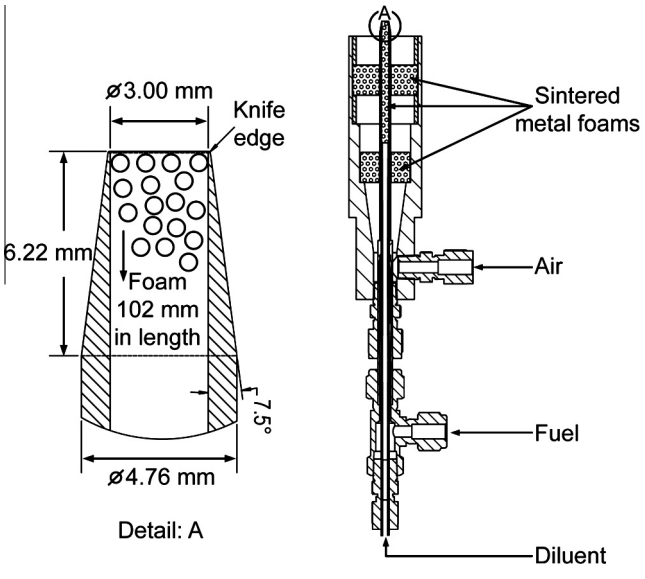

Fig. 2. Details of the liquid fuel burner.

The ratio of fuel flow rate to the amount of dilution was selected by trial and error such that a stable laminar diffusion flame can be obtained at most of the pressures considered, and the carbon flow rate of *n*-heptane would match those of our previous experiments with gaseous fuels. In nitrogen-diluted *n*-heptane experiments, *n*-heptane and nitrogen flow rates were set to 0.49 mg/s and 1.04 mg/s, respectively. This mass flow rate of *n*-heptane corresponds to a carbon flow rate of 0.41 mg/s which matches the carbon flow rates of previous experiments with methane [15], ethane [17], and propane [16]. In addition to nitrogen-diluted flames, we attempted measurements with helium-diluted *n*-heptane flames with the expectation of better flame stability. In helium-diluted *n*-heptane experiments however, the carbon flow criterion could not be satisfied because of unstable flames, and *n*-heptane and helium flow rates were set to 0.29 mg/s and 0.3 mg/s, respectively. Co-flow air was about 0.42 g/s and the line was kept at 475 K. Fuel line to the burner was maintained at about 520–530 K. For each pressure, measurements were obtained at height increments of 0.5 mm from the burner tip to the tip of the flame and at radial increments of 50 μm. At each measurement location 20–30 images of 1 s duration were captured. For a 2.5 mm diameter flame, a complete horizontal scan would require about 50 min plus the time required to move the combustion chamber using the translational stage to the next measurement location. This procedure is repeated with 0.5 mm height increments to cover the whole flame height.

3. Results and discussion

3.1. Nitrogen-diluted n-heptane flames

Still pictures of nitrogen-diluted *n*-heptane diffusion flames at various pressures, up to 10 atm, are shown in Fig. 3. The stability of laminar diffusion flames, especially originating from buoyancy effects, becomes an important issue at elevated pressures due to the increase in Grashoff number which scales with the square of pressure. Further, any small unsteadiness or oscillation in evaporation of the liquid fuel introduces an additional instability component. As a result, it becomes a challenge to stabilize the liquid fuel laminar diffusion flames at pressures above atmospheric for a period long enough to map the whole flame with desired resolution. SSE measurements of a single flame usually take several hours, and the liquid fuel flame may not be stable that long.

The visible flame height of the nitrogen-diluted *n*-heptane flames stayed constant at all pressures as shown in Fig. 3 at a nominal height of about 9.5 mm. Small deviations, for example at 10 atm, are due to flame instabilities. The theoretical value of the flame height of *n*-heptane under the conditions of the current experiments was calculated as 9.2 mm using the expressions proposed by Roper et al. [28]. The tractability of the laminar co-flow flames at elevated pressures is crucial in assessing the influence of pressure on combustion processes such as soot formation. It has been demonstrated that the flame heights are independent of pressure if the fuel mass flow rate is fixed and the flame is buoyancy dominated. Pressure independence then could only be possible if the flame cross-sectional area scales with the inverse of the pressure [29]. The inverse dependence of the flame cross-sectional area on pressure implies that the residence times are independent of the pressure, and measurements can be compared at the same heights above the burner exit. A detailed numerical study of the residence times in laminar co-flow diffusion flames at elevated

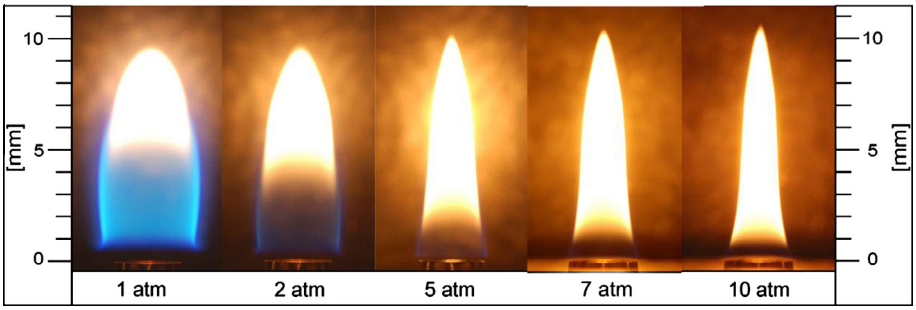

Fig. 3. Still pictures of nitrogen-diluted *n*-heptane flames at various pressures.

pressures can be found in [30]. The first experimental verification of pressure independence of flame height for co-flow flames, albeit within a limited pressure range of 1–1.5 atm, is in the seminal study of diffusion flames by Burke and Schumann [31] in 1928. Visible flame heights of methane–air flames up to 100 atm were shown to have heights that are almost constant at all pressures [6].

The nitrogen diluted *n*-heptane flame exhibited good, long term stability at 5 atm pressure. The root mean square (rms) flicker of the flame tip height was less than 0.2 mm. At 2 and 7 atm, the flames were less stable with an rms flicker up to 0.4 mm. At 1, 3, 8, and 10 atm, the rms flame flicker exceeded 1 mm, and this magnitude of random oscillations prevented to have sound measurements of radially resolved temperature and soot concentrations. At these pressures, there were periods of stable flames lasting typically more than 30 s which is not long enough for measurements with our current diagnostics. Between stable flames, there were long periods of random oscillations lasting several minutes with an rms flicker in excess of 1 mm. As a result, we report measurements at 2, 5 and 7 atm only with nitrogen diluted *n*-heptane flames.

To illustrate the typical fluctuations found in the *n*-heptane–air flames in this experiment, a series of still images captured from a 1-min video clip of the flame at atmospheric pressure is shown in Fig. 4. It is suspected that the cause of these instabilities is in the fuel delivery system, most probably due to small unsteadiness in the evaporation rate of the liquid fuel. It should be noted that, attempts have been made to measure the soot volume fraction at atmospheric pressure, but the signal strength was too low for the SSE system to process properly. This suggests that there was a very low concentration of soot in the *n*-heptane–air flames in this work at atmospheric pressure.

A sample of integrated emission intensity measurements at $P = 2$ atm and HAB = 7.5 mm for a series of chords through the flame is included in Fig. 5. At this height above the burner exit, the emission intensity signal was found to be the highest at $P = 2$ atm. The integrated emission intensity measurements shown in Fig. 5 indicate that the flame has an annular emission structure, and the centreline intensity is about 40–50% lower than the peak

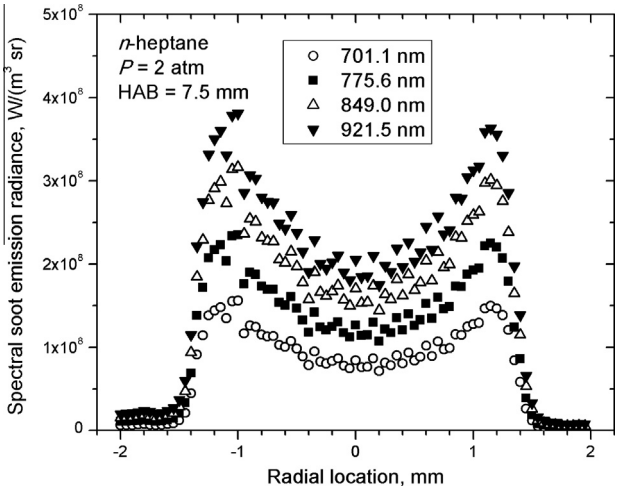

Fig. 5. Line-of-sight soot emission data at 7.5 mm above the burner exit at 2 atm at various wavelengths. Spectra are averaged over the height of the entrance slit as well as across 12 spectral regions, each 25 nm wide. This provides 12 adjacent spectral data points per line-of-sight acquisition. Four of those spectra are shown in the figure.

intensity in the annulus. There is some asymmetry between the two sides of the annulus and the influence of flame oscillations is obvious. The intensity falls rapidly to near zero on either side of the annulus and intensity increases with increasing wavelength.

The integrated emission intensities for the condition of $P = 2$ atm and HAB = 7.5 mm were inverted to obtain the local emission intensities for a series of radial positions. From this information radially resolved soot temperatures and soot volume fractions were calculated using the relationships described previously [14,26]. Briefly, horizontal scans of line-integrated spectra are collected over a spectral range of 690–945 nm. Inversion of these data through one-dimensional tomography using a three-point Abel inversion yields radial distributions of the soot radiation from which temperature profiles are extracted. From an absolute

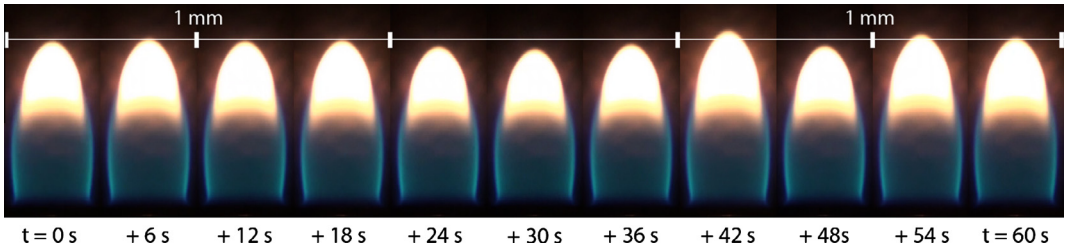

Fig. 4. Series of still images depicting the instability of *n*-heptane–air diffusion flames at atmospheric pressure captured at an interval of 6 s from a 1-min video clip. The length of the vertical scale bar corresponds to 1 mm.

calibration of the flame emission and by use of these temperature data, absorption coefficients are calculated, which are directly proportional to the soot volume fractions [26]. Calculated soot volume fraction and temperature profiles are shown in Fig. 6. The soot volume fraction profile displays the expected annular structure; however the effects of flame oscillations, as well as the relatively low soot emission signal, manifest itself (through the Abel inversion process) as oscillations in the soot volume fraction at radial locations smaller than 1 mm. The radial temperature profile peaks at a larger radial location than the soot volume fraction profile as depicted in Fig. 6. This is consistent with previous observations in ethane diffusion flames [17].

Soot volume fraction profiles at 5 and 7 atm are shown in Figs. 7 and 8, respectively, at several heights above the burner exit. The structure of the soot field is very similar to those reported for gaseous diffusion flames at similar pressures [16,17]. Soot began to form in an annular ring at the height of about 3 mm above the burner exit where the peak soot concentration was about 1.5 ppm, as depicted in Fig. 7. As the height was increased, the peak soot concentration increased and the location of the peak contracted towards the centreline. The soot volume distribution switched from annular profiles to centre peak profiles at the height of 6.5 mm and above. The maximum soot volume fraction at this pressure was found to be 12 ppm at the height of 7.5 mm above the nozzle tip. At heights beyond 7.5 mm, soot concentration decreased as the axial height was increased further towards the flame tip. A similar structure was observed at 7 atm for lower half of the flame as shown in Fig. 8. The data for the upper half of the flame were extremely noisy (rms flicker exceeding 1 mm and lateral side to side random movements) and were omitted from Fig. 8. The maximum soot volume fraction was estimated to be about 32 ppm at 5.5 mm height above the burner exit at 7 atm.

The radial temperature profiles for the *n*-heptane–air flames at 5 atm are shown in Fig. 9 at various heights above the burner exit. The maximum temperature at 5 atm seems to stay slightly below 2000 K. At 7 atm, on the other hand, the maximum temperature is about 100 K lower than that at 5 atm, as shown in Fig. 10. The lower temperatures observed at 7 atm is a manifestation of the higher soot concentrations leading to relatively higher radiative heat losses from the flame. The radial temperature profiles shown in Figs. 9 and 10 are similar to the profiles exhibited by gaseous fuel diffusion flames [15–17].

The sensitivity of the sooting propensity to pressure can be assessed by evaluating the variation of maximum soot yield with pressure. The soot yield is defined as the percentage of total carbon

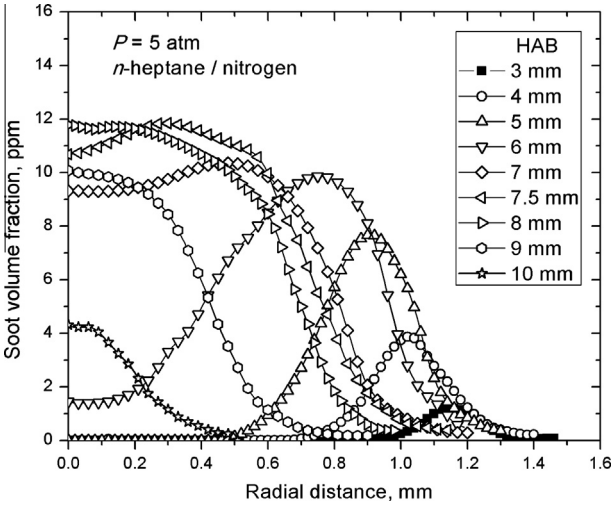

Fig. 7. Radial distributions of soot volume fraction at various heights above the burner exit at 5 atm.

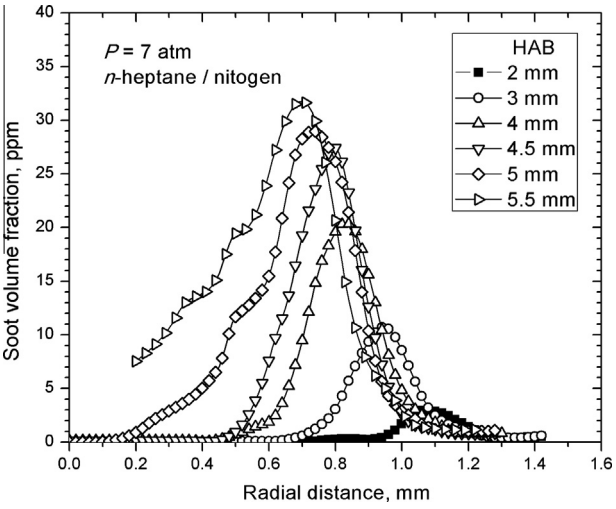

Fig. 8. Radial distributions of soot volume fraction at various heights above the burner exit at 7 atm.

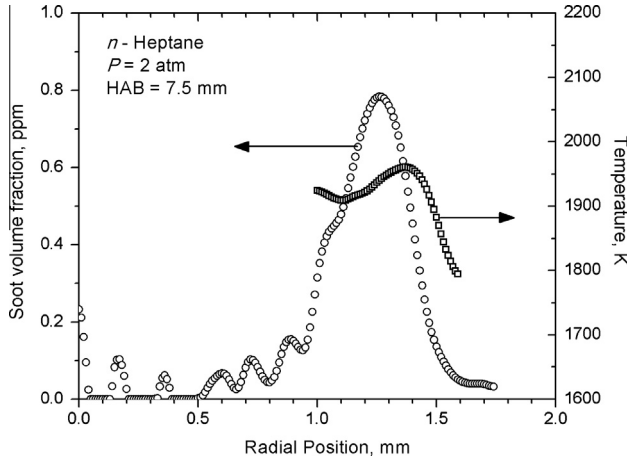

Fig. 6. Radial distributions of soot volume fraction and temperature at 7.5 mm above the burner exit at 2 atm.

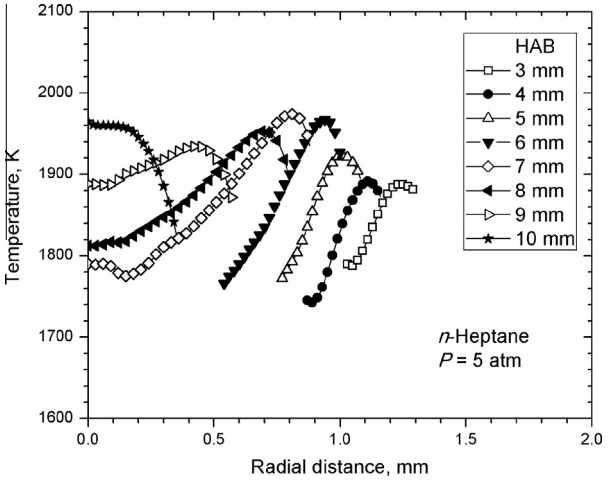

Fig. 9. Radial distributions of temperature at various heights above the burner exit at 5 atm.

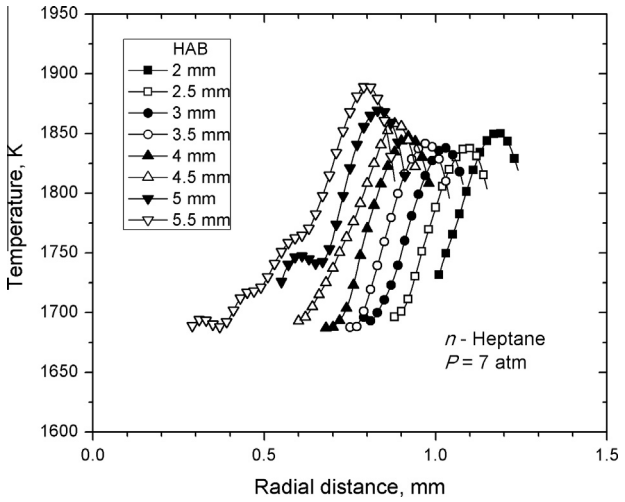

Fig. 10. Radial distributions of temperature at various heights above burner exit at 7 atm.

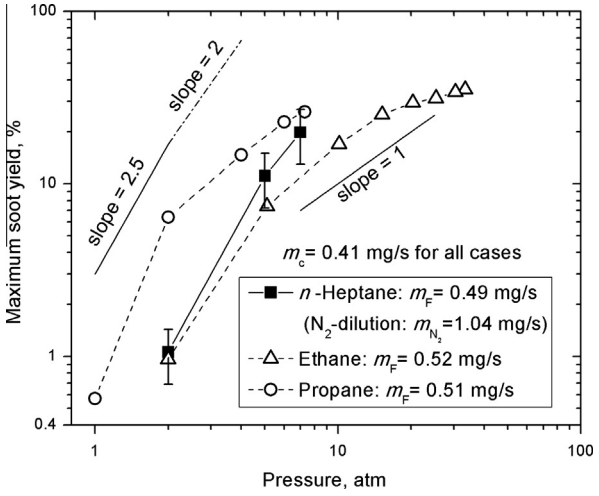

Fig. 11. Maximum soot yield of nitrogen-diluted *n*-heptane flames as a function of pressure. Propane and ethane data from Refs. [16,17], respectively, are included in the plot for comparison of pressure sensitivities. The symbol m_F designates the fuel mass flow rate, and m_c designates the fuel carbon mass flow rate. Note that the soot yields calculated using the computed velocity field were higher than the soot yields calculated using a constant acceleration value by 28% at all pressures.

in the fuel converted to soot. The mass flow rate of carbon, in the form of soot, can be determined through the relationship

$$\dot{m}_s(z) = 2\pi\rho_s \int v_z(r,z) f_v(r,z) r dr \qquad (1)$$

where v_z is the axial velocity, $\rho_s = 1.8$ g/cm^3 is the soot density, f_v is the soot volume fraction, r is the radial coordinate, and z is the axial height. The percentage of carbon in the fuel converted to soot, or the soot yield, is simply $Y_s = \dot{m}_s/\dot{m}_c$ where $\dot{m}_c$ is the carbon mass flow rate at the nozzle exit. The axial velocity could be estimated using the relationship $v_z(z) \approx \sqrt{2az}$, where a is an acceleration constant commonly assumed to be 25 m/s^2 at atmospheric pressure [28]. In recent studies [30,32] it was found that the acceleration constant a, which is used to estimate the axial velocity of the flame as a function of height, is larger than 25 m/s^2 at super-atmospheric pressures. Instead of calculating the soot yield from Eq. (1) using the constant acceleration, the velocity field within the flame envelope computed from a full numerical simulation was used. The maximum soot yield calculated with this approach is shown in Fig. 11. In Fig. 11, a power-law relationship between the percentage conversion of fuel's carbon to soot and the pressure is not obvious and there are only three data points. However, if one seeks a relationship in the form of $Y_s \propto P^n$, the value of exponent n seems to be between 2 and 2.5.

For comparison, our previous soot yield results with ethane and propane are plotted in Fig. 11 along with nitrogen-diluted *n*-heptane soot yields. It should be noted that for all three fuels shown in Fig. 11, the carbon mass flow rates of the fuels are identical and the soot yields have been evaluated using the computed velocity fields. A comparison of the pressure dependencies of the soot yields indicates that *n*-heptane flame seems to be slightly more sensitive to pressure than both ethane and propane flames. However, it should be noted that the *n*-heptane data are limited to three points and such a comparison may not be fully justified. In a recent study [19] originating from the senior author's laboratory, available high-pressure soot yield data from diffusion flames of methane, ethane, and propane were shown to display a unified dependence on reduced pressure when the soot yield is properly scaled. The maximum soot yield was shown to reach a plateau asymptotically as the pressure exceeds the critical pressure of the gaseous fuel [19]. However, it is not possible to see whether the soot yield of *n*-heptane would show a similar dependence on reduced pressure (pressure scaled with the critical pressure of the fuel). In order to carry out this comparison, the effect of nitrogen dilution on soot yield and the variation of this effect, if any, with pressure should be quantified first.

The maximum total uncertainty in soot measurements reported in this work was evaluated as 35%. The error bars in Fig. 11 correspond to this maximum total uncertainty. The total uncertainty in temperature measurements was estimated as 3.5%. These uncertainties are similar to those estimated for our previous measurements using the same measurement techniques with gaseous diffusion flames at high pressures [14–19]. Full details of the methodologies for the uncertainty analysis can be found in [26,33].

3.2. Helium-diluted n-heptane flames

Still pictures of helium-diluted *n*-heptane diffusion flames at various pressures, up to 5 atm, are shown in Fig. 12. The visible flame height of the helium-diluted *n*-heptane flames stayed

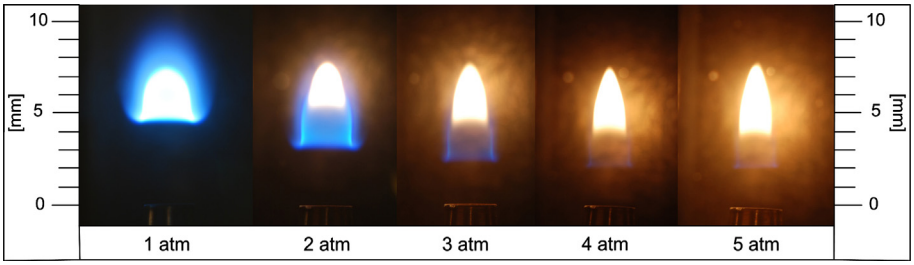

Fig. 12. Still pictures of helium-diluted *n*-heptane flames.

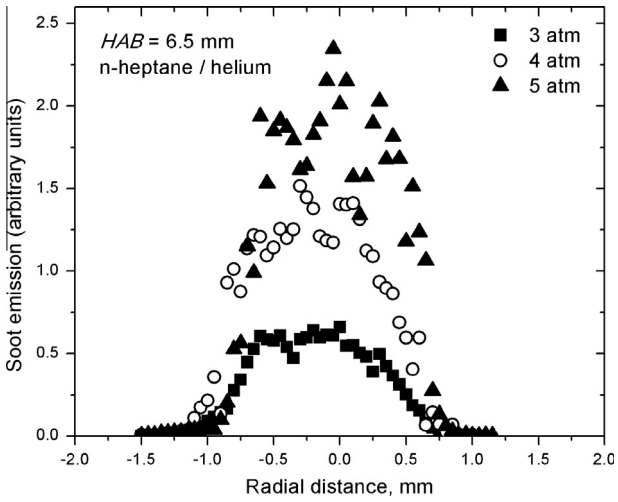

Fig. 13. Soot emission profiles at various pressures at a height of 6.5 mm above the burner exit. Helium-diluted *n*-heptane.

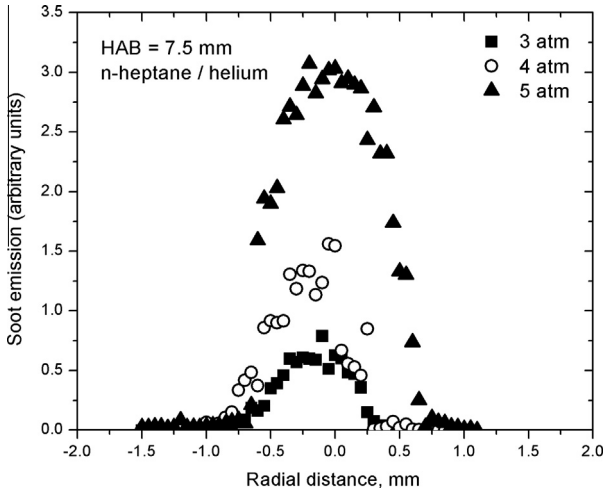

Fig. 14. Soot emission profiles at various pressures at a height of 7.5 mm above the burner exit. Helium-diluted *n*-heptane.

constant at all pressures, as shown in Fig. 12, at a nominal height of about 7.5 mm. Small deviations are due to flame instabilities. The theoretical value of the flame height of *n*-heptane under the conditions of the current experiments with helium dilution was calculated as 6.2 mm using the expressions proposed by Roper et al. [28]. However, it should be noted that helium-diluted flames are lifted, Fig. 12, and they could be more partially premixed rather than pure diffusion flames. Helium-diluted *n*-heptane flames were less stable than nitrogen-diluted ones contrary to the expectations [34]. SSE measurement data obtained at 3, 4, and 5 atm and at two flame heights above the burner exit are shown in Figs. 13 and 14. The noise in the measurements due to flame instabilities prevents a reliable conversion of line of sight SSE data into radially-resolved soot volume fractions by using Abel inversion [27]. Although it is difficult to discuss the pressure sensitivity in helium-diluted *n*-heptane flames quantitatively using the current data, the strong influence of pressure on soot levels is obvious in Figs. 13 and 14.

4. Conclusions

The sooting characteristics of *n*-heptane, diluted with either nitrogen or helium, were measured in tractable laminar diffusion flames at super-atmospheric pressures. The flame stability proved to be a challenge, due to buoyancy effects and instabilities introduced by the evaporation process of the liquid fuel, and stable flames were possible only at certain pressures for a sufficiently long duration to permit measurements. Measured soot volume fraction and temperature profiles in nitrogen-diluted *n*-heptane flames at 2, 5 and 7 atm showed similar trends to those measured in ethane and propane diffusion flames at similar pressures. The limited data provided in this work on the maximum soot yield as a function of pressure in nitrogen-diluted *n*-heptane diffusion flames indicate that *n*-heptane flames are slightly more sensitive to pressure than aliphatic gaseous hydrocarbon flames at least up to 7 atm. Limited measurements of soot intensity from helium-diluted *n*-heptane diffusion flames at 3, 4, and 5 atm were not of desired quality for a quantitative discussion.

Acknowledgments

The authors acknowledge financial support for this work from Natural Sciences and Engineering Research Council of Canada, Canada Foundation for Innovation, and Canadian Space Agency.

References

[1] A. Mensch, R.J. Santoro, T.A. Litzinger, S.-Y. Lee, Combust. Flame 157 (2010) 1097–1105.
[2] Y. Yang, A.L. Boehman, R.J. Santoro, Combust. Flame 149 (2007) 191–205.
[3] D.B. Olson, J.C. Pickens, R.J. Gill, Combust. Flame 62 (1985) 43–60.
[4] Ö.L. Gülder, Combust. Flame 78 (1989) 179–194.
[5] L.M. Li, P.B. Sunderland, Combust. Sci. Technol. 184 (2012) 829–841.
[6] A.E. Karataş, Ö.L. Gülder, Prog. Energy Combust. Sci. 38 (2012) 818–845.
[7] G.M. Faeth, in: H.D. Ross (Ed.), Microgravity Combustion: Fire in Free Fall, Academic Press, 2001, pp. 83–182.
[8] J.B. Moss, in: G. Cox (Ed.), Combustion Fundamentals of Fire, Academic Press, London, 1995, pp. 221–272.
[9] A. Cavaliere, R. Ragucci, Prog. Energy Combust. 27 (2001) 547–585.
[10] C.H. Kim, F. Xu, G.M. Faeth, Combust. Flame 152 (2008) 301–316.
[11] W.L. Flower, C.T. Bowman, Proc. Combust. Inst. 21 (1988) 1115–1124.
[12] W. Lee, Y.D. Na, JSME Int. J. Ser. B 43 (4) (2000) 550–555.
[13] L.L. McCrain, W.L. Roberts, Combust. Flame 140 (2005) 60–69.
[14] K.A. Thomson, Ö.L. Gülder, E.J. Weckman, R.A. Fraser, G.J. Smallwood, D.R. Snelling, Combust. Flame 140 (2005) 222–232.
[15] H.I. Joo, Ö.L. Gülder, Proc. Combust. Inst. 32 (2009) 769–775.
[16] D.S. Bento, K.A. Thomson, Ö.L. Gülder, Combust. Flame 145 (2006) 765–778.
[17] P.M. Mandatori, Ö.L. Gülder, Proc. Combust. Inst. 33 (2011) 577–584.
[18] H.I. Joo, Ö.L. Gülder, Combust. Flame 158 (2011) 416–422.
[19] Ö.L. Gülder, G. Intasopa, H.I. Joo, P.M. Mandatori, D.S. Bento, M.E. Vaillancourt, Combust. Flame 158 (2011) 2037–2044.
[20] H. Gohari Darabkhani, J. Bassi, H.W. Huang, Y. Zhang, Fuel 88 (2009) 264–271.
[21] A.G. Mouis, A. Menon, V. Katta, T.A. Litzinger, M. Linevsky, R.J. Santoro, S.P. Zeppieri, M.B. Colket, W.M. Roquemore, Combust. Flame 159 (2012) 3168–3178.
[22] K. Harstad, J. Bellan, Combust. Flame 157 (2010) 1594–1609.
[23] T. Yuan, L. Zhang, Z. Zhou, M. Xie, L. Ye, F. Qi, J. Phys. Chem. A 115 (2011) 1593–1601.
[24] V.R. Katta, S.K. Aggarwal, W.M. Roquemore, Fuel 93 (2012) 339–350.
[25] I.M. Miller, H.G. Maahs, NASA Technical Paper TN D-8407, 1977.
[26] D.R. Snelling, K.A. Thomson, G.J. Smallwood, O.L. Gülder, E.J. Weckman, R.A. Fraser, AIAA J. 40 (9) (2002) 1789–1795.
[27] J. Dasch, Appl. Opt. 31 (8) (1992) 1146–1152.
[28] F.G. Roper, C. Smith, A.C. Cunningham, Combust. Flame 29 (1977) 227–234.
[29] Glassman, R.A. Yetter, Combustion, fourth ed., Academic Press, 2008.
[30] M.R.J. Charest, C.P.T. Groth, Ö.L. Gülder, Combust. Flame 158 (2011) 1933–1945.
[31] S.P. Burke, T.E.W. Schumann, Ind. Eng. Chem. Res. 20 (1928) 297–318.
[32] M.R.J. Charest, C.P.T. Groth, Ö.L. Gülder, Combust. Flame 158 (2011) 860–875.
[33] K.A. Thomson, PhD Thesis, University of Waterloo, Waterloo, Ontario, Canada, 2005.
[34] F. Lorenzo, A. Gomez, Combust. Flame 159 (2012) 142–150.